Clarke et al. BMC Zoology (2020) 5:5
https://doi.org/10.1186/s40850-020-00054-6

BMC Zoology

RESEARCH ARTICLE Open Access

Sea anemones (*Exaiptasia pallida*) use a secreted adhesive and complex pedal disc morphology for surface attachment

Jessica L. Clarke[1], Peter A. Davey[1] and Nick Aldred[1,2*]

Abstract

Background: The mechanism by which sea anemones attach to surfaces underwater remains elusive, which is surprising given their ubiquitous distribution in the world's oceans and tractability for experimental biology. Their adhesion is mechanically interesting, bridging the interface between very hard and soft materials. The Cnidaria are thought to have evolved adhesion to surfaces at least 505 Ma ago implying that, among the Metazoa, only Porifera developed this capability earlier. The purpose of this study was primarily to address an existing hypothesis, that spirocysts (a sticky class of cnidocyst) facilitate adhesion to surfaces, as observed during prey capture.

Results: We demonstrated conclusively that spirocysts were not involved in the pedal disc adhesion of *Exaiptasia pallida*. Second, we applied a variety of imaging methods to develop an understanding of the true adhesion mechanism. Morphological studies using scanning electron microscopy identified a meshwork of adhesive material, unique to the pedal disc. Serial block-face SEM highlighted four classes of cells that could secrete the adhesive from the pedal disc ectoderm. A variety of histochemical techniques identified proteins, glycans and quinones in the cell contents and secreted adhesive, with variation in contents of specific cell-types in different areas of the body.

Conclusions: Spirocysts are not used by *Exaiptasia pallida* for adhesion to surfaces. Instead, a structurally and compositionally complex secreted glue was observed, firmly attaching the animals underwater. The results of this study provide a basis for further investigations of adhesion in Cnidaria, and establish *E. pallida* as a new model organism for bioadhesion research.

Keywords: Sea anemone, Adhesion, Exaiptasia, Cnidocyst, Spirocyst, Bioadhesion

Background

Sea anemones (Cnidaria, Anthozoa, Actinaria) are common marine invertebrates related to corals, hydrozoans and other jellies. They exist, for the most part, as solitary polyps attached to surfaces and are exclusively marine. Anemones face the same basic challenges met by other sessile marine invertebrates; namely the need to collect food, protect themselves and, perhaps most importantly, remain attached to a surface in the dynamic marine environment. The first requirement is met by cnidocysts. Cnidocysts (nematocysts, spirocysts and pytchocysts) are organelles unique to the cnidocytes of Cnidaria and are used for prey capture [1]. In addition to their role in feeding, venomous nematocysts provide the otherwise vulnerable organism with a defensive mechanism, including inter- and intra-specific aggression, so fulfilling a protective role [2, 3]. The question of how anemones remain attached to surfaces, however, has never been satisfactorily answered.

Literature relating to the use of cnidocysts in pedal disc adhesion is scarce and contradictory [4–6]. It has been proposed that spirocysts (glutinate cnidocysts) could

* Correspondence: nick.aldred@essex.ac.uk
[1]School of Natural and Environmental Sciences, Newcastle University, Newcastle upon Tyne NE1 7RU, UK
[2]School of Life Sciences, University of Essex, Wivenhoe Park, Colchester CO4 3SQ, UK

mediate surface adhesion via ejection of sticky threads at the interface. Indeed, Mcfarlane and Shelton [7] demonstrated a key role for spirocysts in the adhesion of tentacles to surfaces during "shell climbing" behaviour of the epibiotic anemone *Calliactis parasitica*. While the sticky threads [1, 8, 9] contained within spirocysts clearly have an important role in prey capture [9–11], their implied role in more permanent adhesion to surfaces remains highly circumstantial.

There is no doubt that cnidocysts exist in the pedal tissue of anemones, although studies of anthozoan cnidomes have so-far neglected to analyse those present in the pedal disc specifically [1, 12, 13]. Pragmatically, it seems unlikely that ejected threads of cnidocysts (spirocysts or nematocysts) could account alone for the typically tenacious adhesion of anemones to surfaces. For that mechanism to work effectively, there would need to be a large number of specialised adhesive cnidocysts whose threads would need to propagate through the adhesive interface prior to complete attachment. The turnover of the basal tissue would need to be constant, given the transitory nature of adhesion in many anemone species [2, 4, 14] and the 'single use' nature of cnidocysts. An obvious alternative mode of adhesion, either complementary to or instead of the use of cnidocysts, is secretion of a bespoke adhesive material from the tissue of the pedal disc [5, 15, 16]. This secretion could act alone or in combination with specific morphological or behavioural adaptations [17], but would need to be secreted from cells of the basal ectoderm, since cnidarians have only two tissue layers separated by collagenous mesoglea.

To address this fundamental gap in knowledge, we focussed on an emerging model, *Exaiptasia pallida* [18]. *E. pallida* is a fast-growing tropical species with a zooxanthellae symbiosis. It has a typical actinarian body plan, consisting of an aboral pedal disc for attachment to the substratum, a column and an oral disc (mouth) that is encompassed by tentacles armed with spirocysts and nematocysts (Fig. 1). *E. pallida* also have acontia; nematocyst-filled 'threads' that can be used for defence. The trilaminate body wall consists of an endoderm, mesoglea and ectoderm (Fig. 1). The genome of this species has been sequenced [20] and, recently, a transcriptome-based analysis found differentially expressed genes in the pedal disc [19]. Availability of genomic resources, the fast growth and asexual pedal laceration of *E. pallida* make it a tractable model for ecological studies of Anthazoa, as well as an ideal test species for developing fundamental insight into bioadhesion of marine invertebrates. A model species that evolved adhesion to surfaces long ago could provide a basis for studies to identify convergent themes, or components of bioadhesives that have been retained or selected repeatedly by evolution, in the adhesives of distantly-related species. Cnidarians are known to have been sticking to surfaces for much of metazoan evolutionary history. For example, *Mackenzia* spp., an anemone-like cnidarian identified in Burgess Shale fossil records, was frequently found adhered to hard substrata having evolved this capability more than 505 million years BCE [21].

Diverse bioadhesive systems are found throughout the natural world, from prokaryotic organisms [22–25] to eukaryotes that exhibit complex metazoan body plans [25–28]. Bioadhesion processes exhibit variability in mode, composition, function and physico-chemical characteristics [29, 30]. Adhesion-related morphology, behaviour and secretions are thus involved in a diverse array of ecological processes including, but not limited to: attachment to surfaces [15, 31, 32], locomotion [33, 34], prey capture [35, 36], building [37, 38] and defence [39, 40]. In particular, many marine organisms have the ability to create strong temporary or permanent adhesive bonds that work effectively in wet environments of high ionic strength, unlike synthetic adhesives that are often compromised by the presence of water, salt or sub-optimal conditions of pH. Specific interest in marine

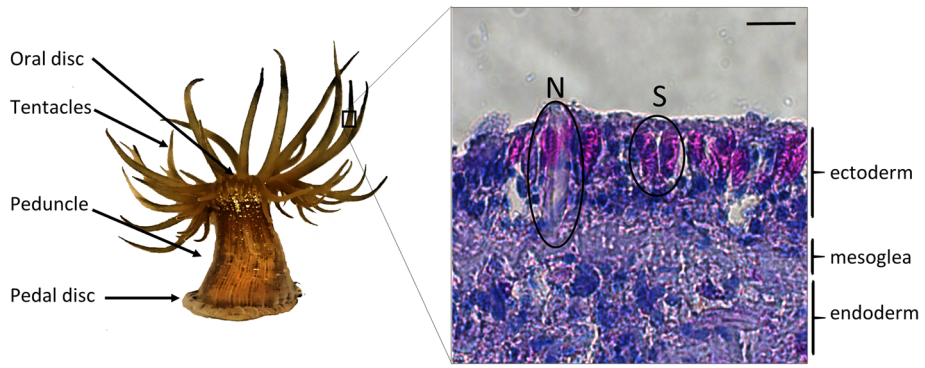

Fig. 1 *Exaiptasia pallida* body plan and tissue from tentacle (image adapted from Davey et al., 2019 [19]). The anemone comprises of an aboral pedal disc, a column and an oral disc (mouth) that is encompassed by tentacles. [Spirocysts (S), Nematocysts (N)]. Scale bar = 10um

bioadhesives has grown in recent years owing to the availability of improved technologies for the analysis and replication of biological materials. It seems realistic, therefore, that the fundamentals of biological adhesion could soon inspire novel medical materials [41], synthetic bonding technologies [42–44], and/or improve the efficacy of fouling-control technologies [45–47]. Bioadhesive secretions are typically composed of proteins, polysaccharides and lipids. Proteins are often post-translationally modified to provide the specific functionality required, including by sulphation, glycosylation, hydroxylation and phosphorylation [29, 48–51]. Composition varies significantly between taxa and between permanent and temporary adhesives. While there are some common themes including the presence of L-dihydroxyphenylalanine (L-DOPA) [37, 48, 52] and phosphorylated serine residues [49, 50] in the adhesive proteins of distantly related species, these are by no means universal.

The objectives of this study were two-fold: The first aim was to establish whether spirocysts or other relevant nematocyst types were present in the pedal disc of *E. pallida* and, if so, whether they were directly involved in adhesion as had been suggested previously. Second, a morphological and histochemical study of the ectoderm was undertaken to highlight physical and/or biochemical features unique to the pedal disc that may point towards adaptation for adhesion.

Results

Absence of spirocysts in the pedal adhesion mechanism

Scanning Electron Microscopy (SEM) of footprints remaining on PVC coverslips after removal of the animal (Fig. 2a), and observation of the pedal disc itself (Fig. 2b), revealed an absence of ejected spirocysts or other nematocyst thread/capsule types at the interface (Fig. 2a,b,c,d). Rather, a thin film of material was present between the anemone and the surface (Fig. 2c). When this material was observed on a surface from which an anemone had been removed, it had the appearance of a structured meshwork (Fig. 2c). Light microscopy imaging of sections identified the presence of undischarged nematocysts in the basal tissue of *E. pallida*, but an absence of spirocysts (Fig. 3a). It is therefore concluded that spirocysts are not a component of the *E. pallida* pedal adhesion system and that the nematocyst types present in the pedal disc do not eject during attachment.

Pedal disc and associated footprint morphology

The body wall of *E. pallida* was externally covered by microvilli (~ 100 nm in diameter), which aggregated into a 'honeycomb'-like structure only on the surface of the pedal disc (Fig. 2e). It has not been determined conclusively if the aggregation of the villi is an adaptation for adhesion, or a consequence of adhesion. Anemones that were imaged before they had completely attached to the surface presented the same aggregation of villi on their

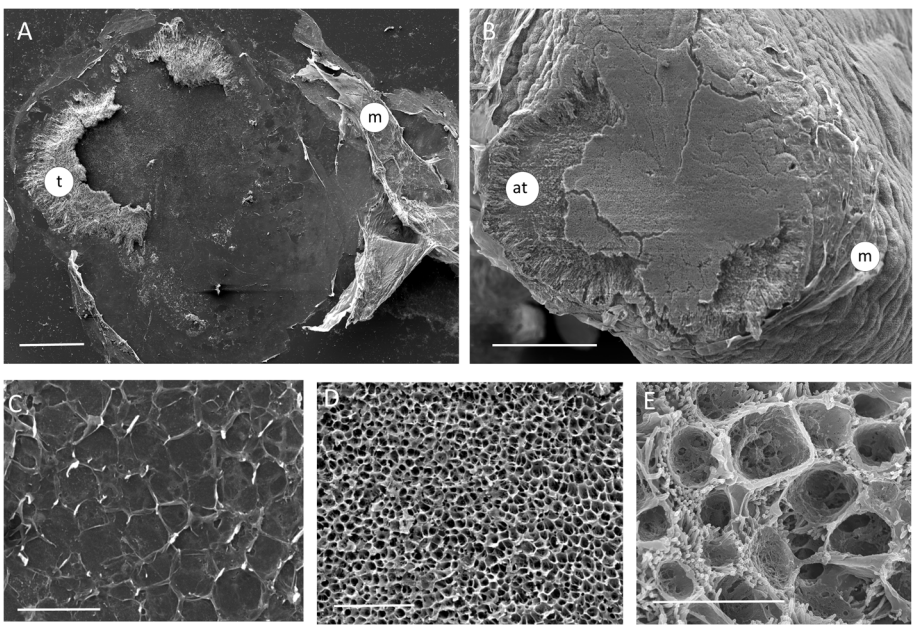

Fig. 2 Scanning electron microscope images of the pedal disc and footprint of an individual attached anemone. **a** A complete footprint with some tissue remaining (t) and mucus secretions (m). **b** A complete pedal disc with some absent tissue (at) that remained on the substratum. External mucus secretions can be seen on the outside of the animal (m). **c** A high magnification image of the secreted footprint, which formed a meshwork between the anemone and the substratum. **d-e** A high magnification image of the pedal disc. Microvilli formed a 'honeycomb'-like structure on the base which corresponded to the meshwork of the footprint. Scale bars: (**a-b**) 200 μm (**c**) 10 μm (**d**) 20 μm (**e**) 5 μm

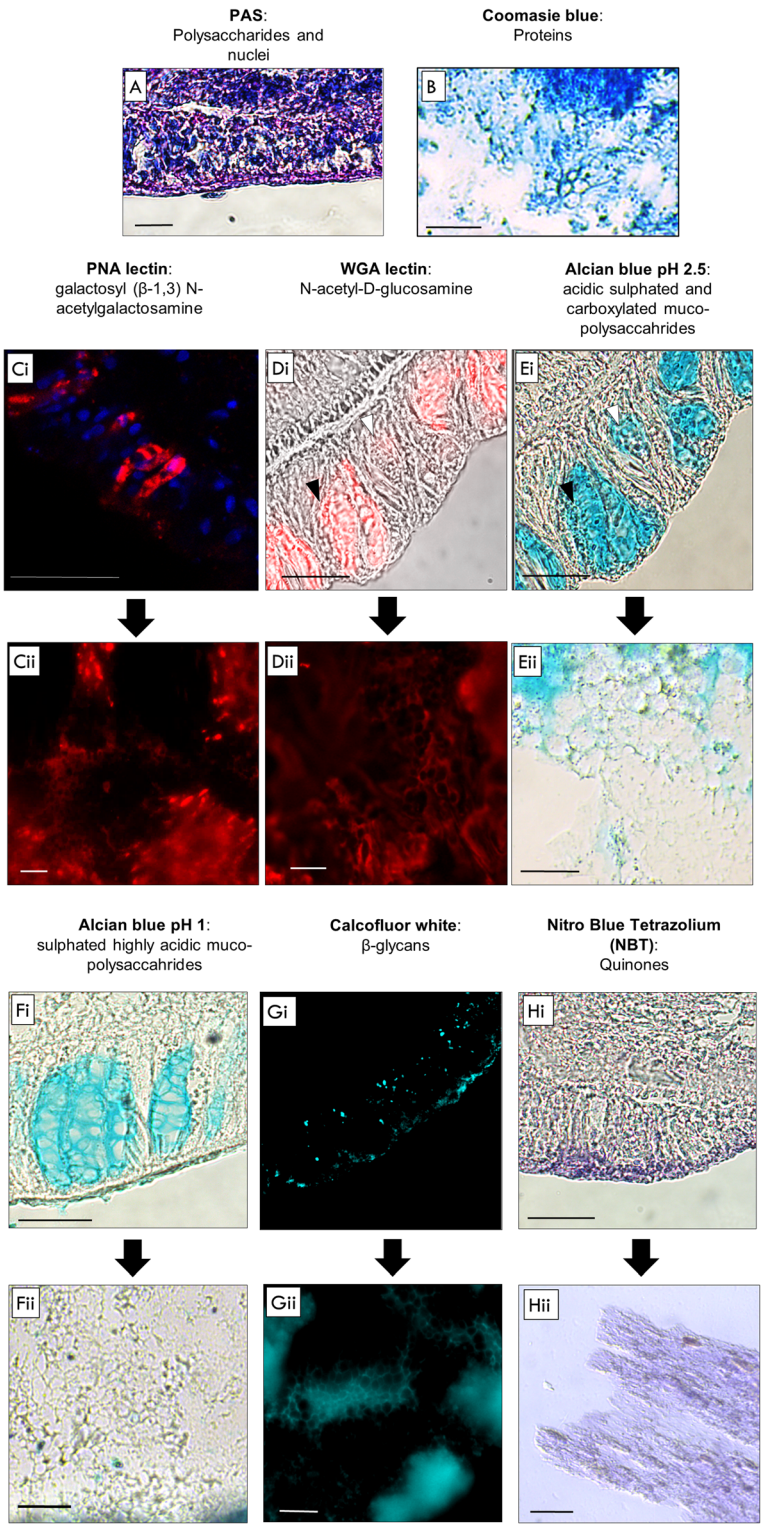

Fig. 3 (See legend on next page.)

(See figure on previous page.)
Fig. 3 Histological staining of the pedal disc (i) and corresponding footprints (ii). (A) PAS and haematoxylin staining. Pink = general polysaccharides, blue = nuclei. Absence of spirocysts within the basal tissue compared to Fig. 1. (B) Footprint strongly stained for protein using Coomasie blue. (C) PNA labelling (red) and nuclei (DAPI: blue). (D) WGA labelling. (Di) Fluorescent and bright field images overlapped. (E) Muco-polysaccharide staining using Alcian blue pH 2.5 (D,E) black arrow indicates cells stained strongly by WGA and Alcian blue pH 2.5. White arrow indicates cell stained strongly with Alcian blue and weakly by WGA. (F) Highly acidic muco-polysaccharides stained using Alcian blue pH 1. (G) β-glycan staining using calcofluor white (Gi is a fluorescent 3D deconvoluted image). (H) Quinone staining using Nitro-Blue Tetrazolium. Scale bars = 20 μm

bases. The corresponding secreted meshwork was not present on the surface until adhesion had been completed, however, suggesting that the structured meshwork on the surface likely resulted from transfer of material from the already aggregated basal villi. The secreted meshwork (Fig. 2c) corresponded well to the morphology of the honeycomb-like aggregation of villi on the pedal disc, the voids of which ranged from 2 to 7 μm in diameter (Fig. 2e). Mucus, which is constantly secreted by *E. pallida* onto their body surface, was clearly distinguishable from the structures described above. Mucus secretions were seen as homogenous films surrounding footprints and on the surface of whole anemones (Fig. 2a,b).

Tissue structure

The outer membrane of the ectoderm was densely populated by microvilli over the entire body surface (Fig. 2e, 4). Nematocysts and secretory cell types were arranged perpendicular to the mesoglea, with their openings at the external surface (Fig. 4a). Four visually distinct cell types, containing vesicular or granular structures, were common throughout the ectoderm. In the absence of functional data we refer to these here simply as types i-iv. In the pedal disc, these cell types all terminated externally at the interface between the anemone and the substrate, suggesting a secretory role.

The largest secretory cell type was consistent with the description of cnidarian mucocytes (cell type i Fig. 4a-c) [53, 54]. These cells contained tightly packed vesicles that varied in appearance within and between cells, from homogenous to highly granular. This variability could indicate different stages of maturity (Fig. 4c). Cells of type ii (Fig. 4c-d) were packed with homogenous and electron lucent vesicles. Cell types iii (Fig. 4a,b,e) and iv (Fig. 4b,f) contained distinct vesicles and, unlike vesicles of type i cells, these were not compacted within the cell. Vesicles within cells of type iii were typically elongated with average lengths of 0.7-1 μm. In cell type iv, the vesicles were spherical in appearance and averaged around 0.4–0.68 μm in diameter. In addition to these four cell types, considered of interest in the context of adhesion, there was a range of other vesicular structures present in the ectoderm, including an abundance of electron dense granular matter located in the apical cytoplasm of the microvilli-bearing cells (Fig. 4a,b,c).

Histochemical analysis of tissues and footprints

The ectoderm of *E. pallida* was heavily populated by putative mucocytes (cell type i). Although there was positive staining of mucosubstances in the ectoderm throughout the animal (Fig. 5), there were noteworthy differences in abundance and appearance of those cells in different locations of the body.

There was abundant staining of mucocytes in the body wall and oral opening but substantially less in the pedal disc using Alcian blue (pH 2.5) (Fig. 5). There was also a distinction between the outer edge of the pedal disc and the central region, with more staining towards the periphery (Fig. 5C vs D). While the outer edge of the pedal disc had the same appearance in tissue structure as the peduncle body wall under these staining conditions, with large mucocytes and large nematocysts present, the central part of the pedal disc exhibited less mucopolysaccharide staining and typically only had small nematocyst types. A thin film was positively stained on the outside of the animal, both on the pedal disc and the body walls, as well as the footprint (Fig. 3 Eii).

Coomasie blue staining confirmed that proteins are a key contributor to the secreted footprint. Proteins were positively identified in the meshwork of the footprint and as a thin film (Fig. 3B) deposited by the pedal disc. Glycans were identified in the footprint and in cellular structures using lectin staining (wheat germ agglutinin (WGA) and peanut agglutinin (PNA)). PNA (detects galactosyl (β-1,3) N-acetylgalactosamine) and WGA (detects N-acetyl-D-glucosamine) both exhibited staining suggestive of 'full' secretory cells throughout the ectoderm. Although this staining was not exclusive to the pedal disc, the film and meshwork of the secreted footprints were nevertheless positively stained.

A 7 μm histology section was stained with Alcian blue pH 2.5, imaged, then subsequently stained with the WGA lectin. Alcian blue (pH 2.5) and WGA showed similar staining patterns (Fig. 3d,e). However, WGA positively stained more specific structures than Alcian blue. Although cells stained by Alcian blue will have some commonality in composition, there was evidently variability in the quantity of N-acetyl-D-glucosamine

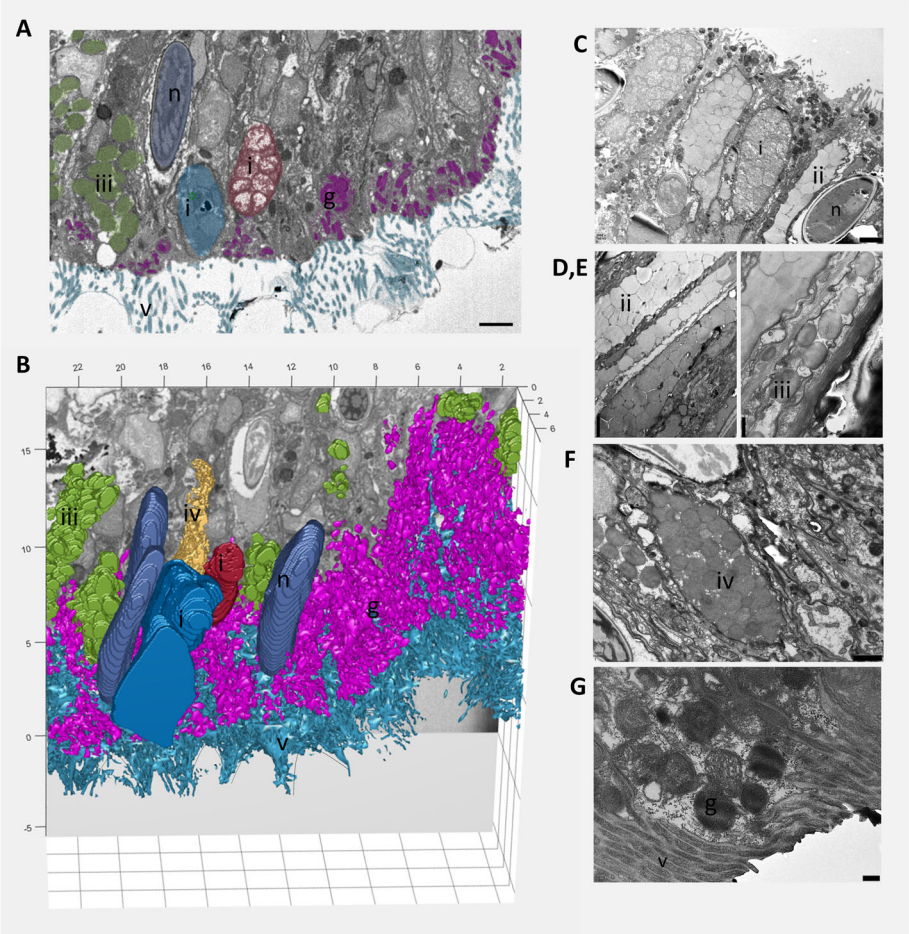

Fig. 4 Putative secretory cell types in the basal tissue of *E. pallida*. **a** 3view serial block-face image and (**b**) rendered 3D isosurface of cell types i – iv (excluding ii, in this image) in the ectoderm of the pedal disc. Cell type i is seen as two variations. One full (blue) vs granular (red). The outer layer of microvilli is also present. n = nematocyst. g = granules. v = villi. **c-g** TEM images of cell types i-iv. n = nematocyst, v = villi, g = granules. **c** High concentration of cell type i and cell type ii in the column of the animal (**d**) cell type ii from the pedal disc. **e** Cell type iii containing distinct vesicles, commonly found in the pedal disc. **f** Cell type iv with small, distinct circular vesicles from the pedal disc. **g** High magnification TEM of the electron dense granular band that runs adjacent and in parallel with the external membrane. Scale bars: (**a**) 2 μm, (**c**) 2 μm, (**d**) 2 μm, (**e**) 500 nm, (**f**) 1 μm, (**g**) 200 nm

present within those cells and this variability was detected by WGA. Alcian blue at pH 1 identified the same cells as at pH 2.5 (Fig. 3E vs F). Staining at pH 1, however, displayed stronger staining around the vesicular membranes compared to their cores. Full cells were only strongly stained at pH 1 in the tentacles and acontia (See Additional file 1), again suggesting variability in the composition of mucocyte contents in different regions of the body. Footprint staining was achieved at pH 2.5, but not at pH 1 (Fig. 3 Eii vs Fii). However, positive staining at pH 1 was achieved in the secreted mucus (See Additional file 1).

β-linked polysaccharide polymers/β-glycans were identified via the fluorescence of calcofluor white. Calcofluor white did not identify the mucocytes highlighted by WGA staining. Therefore, the N-acetyl-D-glucosamine present in the mucocytes was not in the form of chitin. Positive staining with calcofluor white was, however, observed in vesicular structures in between the putative mucocytes as well as staining the meshwork footprint (Fig. 3g). Quinones were positively stained in the secreted footprint film and within the ectoderm as a narrow band parallel with the outer membrane (Fig. 3h).

Discussion

Absence of spirocysts in the surface adhesion mechanism of anemones

Sessile organisms that inhabit dynamic aquatic environments have evolved diverse approaches for adhering to substrata. It seems surprising, therefore, that the adhesion process of anemones has remained almost entirely unstudied given their suitability as experimental organisms.

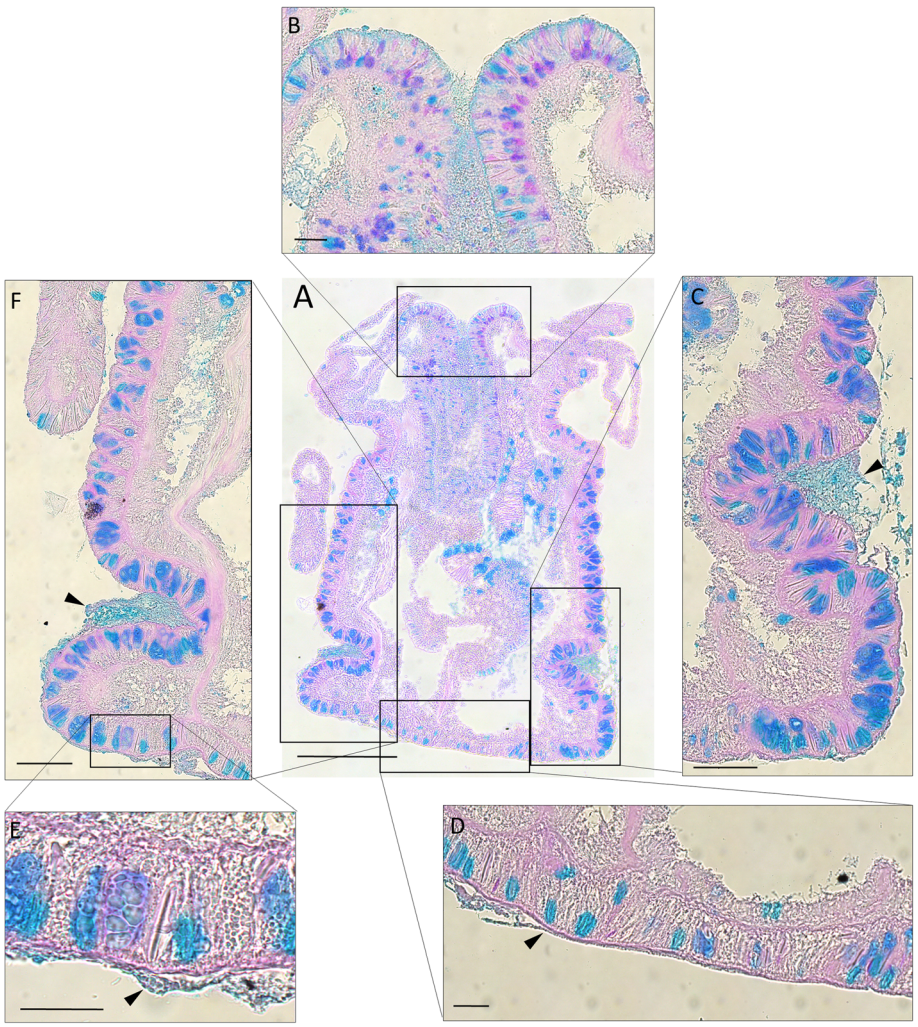

Fig. 5 Tilescan transmitted light images of an Alcian blue (pH 2.5) and PAS stained 7 μm histology section of *E. pallida* (**a-f**). Putative mucocyte abundance and appearance varied depending on location within the body, with the most mucocytes being present in the column (**a, c, f**), and the lowest abundances in the central pedal disc and tentacles (**a** and **d**). The mucocytes identified in the column were large and full (**c** & **f**), whereas those in the pedal disc were smaller in size and number **d**. Arrows indicate externally secreted muco-polysaccharide material. (**a**) 200 μm, (**b**) 20 μm, (**c**) 50 μm, (**d, e**) 20 μm, (**c**) 50 μm

An evolutionarily unique feature of cnidarians is their cnidocytes, or stinging cells. In the context of adhesion, a particular type of cnidocyte, the spirocyst, is used by anemones to catch prey [8, 10, 11] and has thus been implicated in adhesion to surfaces during larval settlement [1, 55] and tentacle walking behaviour [7]. Studies of the anthozoan cnidome have confirmed that cnidocyst types are distributed in a tissue-specific manner, however the adhesive pedal disc has never been specifically targeted by such analyses [1, 12, 13].

Using SEM and histological approaches it was possible to rule out a role for spirocysts and, most likely, any type of nematocyst in the adhesion of *E. pallida* to surfaces. Spirocysts were absent from the pedal disc tissue and the footprint (Fig. 2 a,c & Fig. 3 a), while they were observed in abundance in tentacles and acontia (Fig. 1). The evidence provided here therefore supports the observations of three previous studies in which the role for spirocysts has been contested [5, 16, 56]. It is likely that spirocysts discovered at the adhesive interface in previous studies of anemone adhesion were a result of rough handling of the animals, or the natural process of transitory adhesion engaged in by anemones prior to attachment [16], during which the tentacles are often used. This is not to say that the pedal disc is lacking in nematocysts; far from it. Cnidocytes of various types are abundant, with a prevalence of small types in the pedal disc. They are not discharged during adhesion to surfaces, however, and their purpose has yet to be determined. In a recent differential transcriptomic study of *E.*

pallida [19], genes for 'nematocyst expressed protein 6' and 'golgi-associated plant pathogenesis related protein 1' (GAPR-1) were found to be upregulated in the pedal disc of *E. pallida*. Cnidae arise from a Golgi-microtubule complex [57], therefore the combination of the upregulation of a nematocyst gene and GAPR-1, which is a cysteine-rich secretory protein, led to the speculation that an atypical gland-like nematocyst could play a role in pedal disc adhesion of *E. pallida* [57].

Morphology of the adhesive pedal disc and footprint

The body surface of *E. pallida* was covered by microvilli. Only on the pedal disc, however, did these microvilli aggregate to form a honeycomb-like appearance (Fig. 2e). This complex surface morphology produced a complementary pattern on the surface to which it was attached (Fig. 2c); a secreted meshwork of adhesive which is, presumably, the true means of surface attachment. Microvilli are commonplace in the adhesion apparatus' of diverse organisms. The tail plate of *M. ligano* has a dense array of microvilli, forming part of the adhesive papilla [33]. Barnacle cyprids have dense microvilli on their antenullar discs, which are used for temporary adhesion to surfaces [58]. Adhesive villi have even been identified surrounding the suction disk of the clingfish [26], where they are critical for adhesion to surfaces. Remarkably, the scale of these features is similar in all cases where data are available, with the microvilli of *E. pallida* having diameters of ~ 0.1 μm, which is similar to those of clingfish (~ 0.2 μm), geckos (~ 0.29 μm), and flatworms (~ 0.12 μm) [26, 59, 60].

In cnidarian species where microvilli are apparently not present, for example *Hydra sp*, the footprint meshwork is formed by the contour of individual smooth cells as well as pores in between basal disc cells [15]. Similarly, footprint meshworks have been observed in the adhesive footprints of sea stars, where pores on the surface of the tube feet secrete spheroidal structures, meshwork and a "homogenous film" for adhesion [61]. Finally, the footprints deposited during surface exploration by the cyprid of the barnacle *Semibalanus balanoides* also have the appearance of a meshwork [62]. It is perhaps noteworthy that in the aforementioned adhesion systems are all transitory, or reversible. This is also the case for *E. pallida* which, despite forming a tenacious attachment to a surface, is perfectly capable of locomotion. Whether the meshwork morphology is a consequence of the adhesive delivery mechanism in these instances or confers mechanical advantage to the adhesive/de-adhesive mechanism remains unclear.

Putative adhesive components in the tissue of the pedal disc

It is clear from these results that pedal disc adhesion by *E. pallida* relies on material secreted from the ectoderm of the pedal disc. The structure of the ectoderm was convoluted and putative secretory cells were abundant. Serial block face imaging of a section of the pedal disc allowed for the 3D visualisation of four common cell types that indicated potential secretory roles (Fig. 4). Cell type i clearly corresponded with cnidarian mucocytes, and these were found throughout the ectoderm. Cell types ii and iii, also exhibited secretory potential, containing distinct vesicles and a gland-like structure. There was also a high concentration of relatively small electron-dense granules in the apical cytoplasm, of the microvilli-bearing cells of the ectoderm (Fig. 4). These granules were observed to protrude from the body wall in serial block face images, indicating their secretion. These granules were not exclusive to the base, however, and therefore presumably not specific to pedal disc adhesion. This feature has previously been described in *Calliactis tricolor* [56] and *Metridium sp.*, located in 'supporting cells', and were suggested to be involved in adhesion [5]. These supporting cells are likely to be present in *E. pallida*, however due to the convoluted nature of the tissue, it was hard to distinguish cell types from TEM images. Further study using tissue dissociation would elucidate this. A relationship between similarly described electron dense granules and adhesion has also been suggested for *Hydra* [15]. In non-cnidarians, the flatworm *Macrostomum lignano* exhibits a concentration of electron dense granules called ultrarhabdites along the outer edge of the ectoderm [33]. Rhabdites are rod-shaped secretory products and are thought to form the viscous mucus used in locomotion by ciliary gliding and adhesion [63].

Footprint secretion composition

Young et al. [16] observed strong staining for proteins in surface smears produced by the pedal disc of the anemones *Actinia equina* and *Metridium senile*, and reduced staining in smears of the mucus secreted from the body wall. They were therefore among the first to speculate on the secretion, by anemones, of a specific protein-based adhesive substance. Adhesive proteins are often subject to post-translation modifications (PTMs) [29, 48, 49, 64, 65] including glycosylation [66]. Glycoproteins have been identified in the adhesives of several marine organisms, for example barnacles [67], mussels [68], sea star *Asterias rubens* [34], and the green alga *Ulva sp.* [69]. In *E. pallida,* genes upregulated in the pedal disc suggest that glycosylation may be prevalent in the location of adhesion [19]. Glycosylated proteins were identified in the footprint meshwork and in secretory cells within the ectoderm using lectins (Fig. 3c, d), the purpose of which was to identify components unique, or relatively more abundant, in the pedal disc.

The lectin PNA binds preferentially to galactosyl (β-1, 3) N-acetylgalactosamine residues in glycoconjugates (according to manufacturer's information; Vector Laboratories), and positively labelled secretory cells in *E. pallida*. Lectin staining in *E. pallida* did not provide staining exclusive to the pedal disc, but staining was nonetheless present in the secreted footprint and meshwork, implicating the PNA target in adhesion (Fig. 5c). In the flatworm *Macrostomum lignano,* PNA worked as an adhesive gland cell marker [70, 71]. The lectin WGA binds to N-acetylglucosamine (according to manufacturer's information; Vector Laboratories), which is a dominant residue in the oligosaccharide component of coral mucus [53, 72], as well as the adhesive cells of *Schmidtea mediterranea* [73], *Macrostomum lignano* [70], and the adhesive cells and footprint of *Asterias rubens* [34]. The structures identified by WGA in *E. pallida* correlate to mucocytes, which were found throughout the whole animal but varied in appearance depending on their location in the body (Fig. 4). Although putative mucocytes identified by WGA were reduced in the pedal disc, and SEM investigation showed that the body wall mucous and adhesive differed, the secreted footprint meshwork was nevertheless labelled by WGA (Fig. 5d). Again, this suggested a contribution to adhesion by the contents of the mucocytes. While WGA identifies N-acetyl-D-glucosamine present in small numbers or as a chitin polymer, calcofluor white will only identify chitin polymers and other β-glycans. The fact that these two staining methods did not provide overlapping results (Fig. D vs G) suggests that N-acetyl-D-glucosamine is present, as are unspecified β-glycans, but not in the form of chitin. β-glycans were, however, positively stained in the glutinate spirocysts that had been discharged during manipulation and in the tentacles. Vesicles within the ectoderm and the secreted meshwork of the footprint were both positively stained for β-glycans, implying a role for the β-glycan complexes in adhesion.

Sulphated polysaccharides have been identified in adhesive secretions of other marine invertebrates, for example starfish and tubeworms [64]. Staining of polysaccharide components with Alcian blue is pH dependant. At pH 1, highly acidic sulphated groups are positively identified, whereas as at pH 2.5, acidic sulphated and carboxyl groups are identified. In *E. pallida*, Alcian blue at pH 2.5 stained the same, plus additional cells as identified by WGA, as well as the secreted footprint (Fig. 5d, e). This was also the case at pH 1 in the tissue samples. Staining at pH 1 was much weaker in the base and body walls, with stronger staining around the vesicular membranes within putative mucocytes (Fig. 5f), but strong and 'full' staining of mucocytes in the tentacles and acontia. The footprint meshwork specifically, however, was not positively stained at pH 1 (Fig. 5 Fii). Strong staining of externally secreted mucus was achieved under both pH conditions. This variance between staining conditions suggests compositional differences between mucocytes in different locations e.g. tentacles vs body and base.

Quino-proteins, in particular those containing DOPA, have been at the forefront of bioadhesion research and are documented to play a critical role in several marine species (e.g. mussels [31, 48];, polychaetes [37, 74]; and a hydrozoan [75]). Quino-proteins were positively identified in this study in a narrow band along the ectoderm (Fig. 3h), and in the adhesive footprint. This distribution correlates with that of the electron dense granules found using SBF-SEM (Fig. 4a, g). Although these quinones were not exclusive to the pedal disc, there was stronger and more distinct staining in the pedal disc ectoderm (See Additional file 2), as well as the thin film of the secreted footprint suggesting that quinones may play a role in pedal adhesion.

Conclusions

It is clear from the results of this study that spirocysts do not play a role in pedal disc adhesion of *E. pallida*. Rather, the pedal disc secretes a protein-rich adhesive that is both structurally and compositionally complex. It appears as a meshwork, embedding the honeycomb-like covering of microvilli present on the pedal disc. The adhesive secretion contains quinones and polysaccharides (sulphated, carboxylated and β-glycans), possibly as modifications of proteins and therefore shares similarities with adhesives of distantly-related marine invertebrates. Four cell types were identified in the basal ectoderm that could potentially contribute these components, providing a basis for more penetrating studies of those cells using proteomics and RNA-Seq. Histochemical analysis alone did not, and probably cannot, identify specific cell types exclusive to the pedal disc. It was clear that within these four broad classes of cells there were differences in composition in different regions of the body, and a potentially fruitful next step may be to use these or other staining approaches for cell-sorting of tissues from the pedal disc and column, with differences within cell-types at the transcriptional or protein levels providing more direct identification of biomolecules involved in the adhesion of *E. pallida.*

Methods

Study animals and maintenance

Study animals of *Exaiptasia pallida* [18] (Strain CC007) were originally provided by Dr. Annika Guse at the University of Heidelberg, Germany. The stock cultures were kept in polycarbonate 5-L containers in incubators (LMS ltd, Sevenoaks, Kent) at 26 °C on a 12 h:12 h light

cycle, in 35 ppt artificial seawater (TropicMarin™, Wartenberg, Germany). Individuals used in this study were generated via asexual propagation of lacerates, the rate of which can be increased by regular feeding with freshly hatched *Artemia* (Varicon Aqua Solutions, Hallow UK). For histology samples, 'bleached' animals were used (those that had expelled their symbiotic algae, *Symbiodinium*). To induce bleaching, animals were subjected to cold water shock at 4 °C for 4 hours. Water was replaced with fresh artificial seawater and returned to 26 °C in the dark. Animals were starved for 48 h prior to selection.

Scanning electron microscopy (SEM)

E. pallida were settled on PVC coverslips for 6 h. Following attachment, anemones were anaesthetized in 7.14% $MgCl_2$, (Sigma-Aldrich, Darmstadt, Germany), and fixed in 4% Glutaraldehyde (Fisher Scientific, UK) in phosphate buffered saline (PBS; pH 7.2) for 24 h at 4 °C. Samples were washed several times in PBS to wash off fixative before being processed through a dehydration series of; 50, 70, 90 and 100% absolute ethanol (Fisher Scientific, UK). Samples were chemically dried using Hexamethyldisilizane (HDMS) (Sigma-Aldrich, Darmstadt, Germany) in the following stages at 20 min per stage: 1:2 HDMS:100% ethanol, 2:1 HDMS:100% ethanol, 100% HDMS, a final round of 100% HDMS, and then left to evaporate and dry completely. Samples were mounted onto stubs using black carbon tape with the cover slip attached, at which point the anemone was removed by gently nudging with forceps and mounted onto another stub, tentacles down. Samples were sputter coated (Emitech Sputter Coater) with gold before being examined using a Tescan Vega LMU Scanning Electron Microscope, housed within EM Research Services, Newcastle University. Digital images were collected with Tescan supplied software. High power SEM images were obtained using a FEI SEM Helios Nanolab 600 housed within the Institute of Physics, University of Tartu, Estonia.

Histology and histochemistry

Anemones were settled on Parafilm® for a minimum of 24 h. Following attachment, anemones were anaesthetized in 7.14% $MgCl_2$ and fixed in 4% paraformaldehyde (Sigma-Aldrich, Darmstadt, Germany) in PBS (pH 7.2) for 24 h at 4 °C. Samples were dehydrated in an ascending ethanol series as described in the previous section, and embedded in paraffin. Three individual anemones were embedded per block, and serial sections of 7 μm were obtained using a microtome. Prior to any histological staining, all slides were deparaffinised in two 5-min washes of xylene (Sigma-Aldrich, Darmstadt, Germany) and rehydrated in a descending alcohol series (100, 95, 70 & 50%) to deionized (DI) water. All staining procedures took place at room temperature (RT).

Adhesive footprints were obtained by allowing anemones to attach to glass coverslips for 6–24 h. To reduce agitation and the discharge of mucus, nematocysts and spirocysts when removing live animals from surfaces, attached individuals were anesthetised with 7.14% $MgCl_2$ and fixed with 4% paraformaldehyde in PBS before being carefully detached, leaving the adhesive footprint on the surface.

Samples for histology were stained initially with haematoxylin (Sigma-Aldrich, Darmstadt, Germany) for 90 s, then washed in running tap water for 5 min. Slides were then stained with Eosin Y (Sigma-Aldrich, Darmstadt, Germany) (1%(w/v) in 80% ethanol and one drop of glacial acetic acid (Fisher Scientific, UK). Samples were washed in tap water for 3 min, then DI water before imaging. Footprint samples and additional histology sections were stained with 0.5% (w/v) Alcian Blue 8GX (Sigma-Aldrich, Darmstadt, Germany) in 3% (v/v) acetic acid (pH 2.5) to detect acidic sulphated and carboxylated muco-polysaccahrides, and 1% (w/v) Alcian Blue 8GX in 0.1 N HCl (pH 1) for sulphated highly acidic muco-polysaccahrides. Periodic acid Schiff (PAS) was used as per the manufacturer's instructions (Sigma PAS staining system kit, Sigma-Aldrich, Darmstadt, Germany) to detect neutral polysaccharides and was applied alongside the Alcian blue pH 2.5 stain in histology sections. Quinone staining using nitroblue tetrazolium (NBT) was adapted from Paz et al. [76]. Sections were incubated in 0.24 mM NBT (Sigma-Aldrich, Darmstadt, Germany) in 2 M sodium glycinate (pH 10) (Sigma-Aldrich, Darmstadt, Germany) for 1 h in the dark at RT. The reaction was stopped by placing slides in 1 M sodium borate buffer solution pH 10. Calcofluor white (Cyanamid Co, New Jersey, US) staining was used to detect β-glycans. A 1% (w/v) calcofluor white stock solution was prepared in DI water. For a working concentration, the stock was diluted 10x in DI water and dropped onto the sample slides for 2 min. Samples were washed thoroughly with DI water. General protein was detected in the footprints using Coomasie blue-G solution, prepared as described in Candiano et al. [77]. Samples were stained overnight and then destained for 30mins in a destain solution of 10% phosphoric acid and 20% methanol, rinsed and kept in DI water before imaging. All stained samples were viewed using brightfield, differential interference contrast (DIC) and fluorescence imaging modes on an inverted Leica DMi8 microscope. Images of Calcofluor white-stained samples were obtained using fluorescence microscopy with the DAPI filter set. Images were processed using the Leica LASX software (Leica micro-systems, Milton Keynes, UK).

Lectin-based detection of protein glycosylation

Anemones were settled on Parafilm® for 6–24 h to allow for adequate attachment, anesthetised with 7.14% $MgCl_2$ and fixed in 4% paraformaldehyde in PBS. Individuals

were carefully removed from the surface and embedded in 3% agarose in PBS. Sections of 120 μm were obtained from the agarose blocks using a Vibratome (Camden Instruments Ltd., Loughborough) and were subsequently floated and stored in PBS. Footprints were prepared as described above. Prior to lectin staining, sections were incubated in blocking buffer of 3% BSA-TBS-Tween 0.5%(+ 5 mM $CaCl_2$) (Sigma-Aldrich, Darmstadt, Germany) over-night. Wheat germ agglutinin (WGA) and peanut agglutinin (PNA) were used in this study (Biotinylated lectin kit I, Vector Laboratories Inc., Burlingame, CA). Samples stained with PNA were incubated in blocking buffer supplemented with 5 mM of MnCl. Samples were incubated in the lectin solution at a concentration of 2.5 $\mu L.mL^{-1}$ (in 3% BSA-TBS-T 0.5%(+ 5 mM $CaCl_2$)) for 2 h in the dark at RT. Samples were washed for 15mins six times in TBS-T before being incubated in a solution of streptavidin Texas Red (Vector Laboratories Inc., Burlingame, CA) at a concentration of 1:1000 (in 3% BSA-TBS-T0.5% (+ 5 mM $CaCl_2$)). Samples were washed for 15mins six times in TBS-T before being stained with Phalloidin (for detecting actin) (Molecular Probes, ThermoFisher Scientific, UK) and Hoechst (for detecting nuclei) (ThermoFisher Scientific, UK) with wash stages in-between each stain. Images were acquired using an inverted Leica DMi8 microscope for histological samples and footprints, as well as a Leica SP8 spectral confocal microscope for histological samples. The Hoescht stain was detected using a DAPI filter set. Phalloidin staining was detected using a FITC filter set and lectin staining was detected using the Texas Red filter set.

Transmission electron microscopy (TEM) and serial block-face SEM (SBF-SEM)

Anemones were settled onto Parafilm® for a minimum of 6–24 h, anesthetised with $MgCl_2$ and fixed overnight in 2% glutaraldehyde in 0.1 M sodium cacodylate buffer (TAAB Lab. Equip, Berks, UK). Once fixed, individuals were carefully removed from the Parafilm®. The samples were processed using the heavy metal staining protocol adapted from [78]. Samples were incubated in a series of heavy metal solutions of 3% potassium ferrocyanide in 2% osmium tetroxide (Agar Scientific, Essex, UK), 10% thiocarbohydrazide, 2% osmium tetroxide again, 1% uranyl acetate (Leica ltd, UK) overnight, and finally lead aspartate solution (Leica ltd, UK). Samples were rinsed thoroughly in several changes of DI water between each step. Samples were dehydrated through a graded series of acetone and then impregnated with increasing concentrations of Taab 812 hard resin (Taab Lab. Equip, Berks, UK), with several changes of 100% resin. The samples were embedded in 100% resin and left to polymerise at 60 °C for a minimum of 36 h. The resin blocks were trimmed to approximately 0.75 mm by 0.5 mm and glued onto an aluminium pin. In order to reduce sample charging within the SEM, the block was painted with Achesons Silver Dag (Agar Scientific, Essex, UK) and sputter-coated with a 5 nm layer of gold using a Polaron SEM Coating Unit (Quorum Technologies ltd, East Sussex, UK). The pin was placed into a Zeiss Sigma SEM incorporating the Gatan 3view system, which allows sectioning of the block in situ, and the collection of a series of images in the z-direction. Images were obtained from the pedal disc and the body wall of the anemone at 1.2 k magnification, 2500 × 2500 pixel scan, which gave a pixel resolution of approximately 25 nm. Section thickness was 100 nm in the z-direction. In the resulting z-stacks, glandular and vesicular structures were identified and segmented manually using Microscopy Image Browser (MIB, University of Helsinki) and rendered through Matlab (2017). TEM images were obtained using the same sample block as for the SBF-SEM. Ultrathin sections (70 nm approx.) were cut using a diamond knife on a Leica EM UC7 ultra microtome. The sections were stretched with chloroform mounted on Pioloform-filmed copper grids. The grids are examined on a Hitachi HT7800 transmission electron microscope using an Emsis Xarosa camera with Radius software. (Electron Microscopy Research Services, Newcastle University).

Supplementary information

Supplementary information accompanies this paper at https://doi.org/10.1186/s40850-020-00054-6.

Additional file 1. Alcian blue pH 1 staining of a 7 μm *E. pallida* section.

Additional file 2. NBT staining of a 7 μm *E. pallida* section.

Abbreviations

SEM: Scanning electron microscopy; SBF-SEM: Serial block face - Scanning electron microscopy; TEM: Transmission electron microscopy; DOPA: Dihydroxyphenylalanine; PVC: Polyvinyl chloride; PNA: Peanut agglutinin; WGA: Wheat germ agglutinin; PTM: Post –translational modifications; PBS: Phosphate buffered saline; HDMS: Hexamethyldisilizane; NBT: Nitro-blue tetrazolium

Acknowledgments

We thank Newcastle University's Electron Microscopy Research Services for their expertise and help with preparing samples for SBF-SEM (grant: BB/M012093/1) and TEM (grant: BB/R013942/1) analyses. Rosana Rodrigues of the Universidade de Vigo, Spain, prepared slides for histology. We also thank the EU COST Action ENBA (CA15216) and Dr. Sergei Vlassov for organising an SEM and AFM workshop where high resolution SEM images were obtained.

Authors' contributions

NA designed and received funding for the project. JC performed the laboratory research and drafted the paper. PD and NA assisted and the preparation of the manuscript. The authors read and approved the final manuscript.

Funding

This work was supported by The Leverhulme Trust (Research Project Grant RPG-2017-017). The funder had no role in the preparation of the paper.

Availability of data and materials
Data sharing is not applicable to this article as no datasets were generated or analysed during the study. The images used to draw conclusions are presented in the manuscript and supplemental materials without any manipulations beyond small adjustments to brightness and contrast.

Ethics approval and consent to participate
Not Applicable.

Consent for publication
Not Applicable.

Competing interests
The authors declare that they have no competing interests.

Received: 6 January 2020 Accepted: 21 May 2020
Published online: 05 June 2020

References

1. Strömberg SM, Östman C. The cnidome and internal morphology of *Lophelia pertusa* (Linnaeus, 1758) (Cnidaria, Anthozoa). Acta Zool. 2017;98:191–213.
2. Edmunds M, Potts GW, Swinfen RC, Waters VL. Defensive behaviour of sea anemones in response to predation by the opisthobranch mollusc *Aeolidia papillosa* (L.). J Mar Biol Assoc United Kingdom. 1976;56:65–83.
3. Schlesinger A, Zlotkin E, Kramarsky-Winter E, Loya Y. Cnidarian internal stinging mechanism. Proc Biol Sci. 2009;276:1063–7.
4. Ellis VL, Ross DM, Sutton L. The pedal disc of the swimming sea anemone *Stomphia coccinea* during detachment, swimming, and resettlement. Can J Zool. 1969;47:333–42.
5. Robson EA. Locomotion in Sea Anemones: The Pedal Disk. In: Mackie GO, editors. Coelenterate Ecology and Behavior. Boston: Springer; 1976. p. 479–90.
6. Lawn ID, Mcfarlane ID. Control of shell settling in the swimming sea anemone *Stomphia coccinea*. J Exp Biol. 1976;64:419–29.
7. Mcfarlane D, Shelton G. The nature of the adhesion of tentacles to shells during shell-climbing in the sea anemone *Calliactis parasitica* (couch). J Exp Mar Biol Ecol. 1975;19:177–86.
8. Mariscal RN, McLean RB, Hand C. The form and function of cnidarian spirocysts. Cell Tissue Res. 1977;178:427–33.
9. Mariscal RN, Conklin EJ, Bigger CH. The ptychocyst, a major new category of cnida used in tube construction by a cerianthid anemone. Biol Bull. 1977;152:392–405.
10. Ewer RF, Fox HM. On the functions and mode of action of the nematocysts of *Hydra*. J Zool. 1947;117:365–76.
11. Conklin EJ, Mariscal RN. Increase in nematocyst and spirocyst discharge in a sea anemone in response to mechanical stimulation. In: Mackie GO, editor. Coelenterate ecology and behavior. Boston: Springer; 1976. p. 549–50.
12. Sinniger F, Ocaña OV, Baco AR. Diversity of zoanthids (Anthozoa: Hexacorallia) on Hawaiian seamounts: description of the Hawaiian gold coral and additional zoanthids. PLoS One. 2013;8:e52607.
13. Carlgren O. A contribution to the knowledge of the structure and distribution of cnidae in the Anthozoa. Lunds Univ Arksskr Avd 2. 1940;36:1–62.
14. Lawn ID, Ross DM. The release of the pedal disk in an undescribed species of *Tealia* (Anthozoa: Actiniaria). Biol Bull. 1982;163:188–96.
15. Rodrigues M, Leclère P, Flammang P, Hess MW, Salvenmoser W, Hobmayer B, et al. The cellular basis of bioadhesion of the freshwater polyp *Hydra*. BMC Zool. 2016;1:3.
16. Young GA, Yule AB, Walker G. Adhesion in the sea anemones *Actinia equina* L. and *Metridium senile* (L.). Biofouling. 1988;1:137–46.
17. Van Hemmen A, Ditsche P. Attachment forces and the role of suction in the sea anemone. *Metridium farcimen*. 2014:1–16.
18. Grajales A, Rodríguez E. Morphological revision of the genus *Aiptasia* and the family *Aiptasiidae* (Cnidaria, Actiniaria, Metridioidea). Zootaxa. 2014;3826:55–100.
19. Davey PA, Rodrigues M, Clarke JL, Aldred N. Transcriptional characterisation of the *Exaiptasia pallida* pedal disc. BMC Genomics. 2019;20:1–15.
20. Baumgarten S, Simakov O, Esherick LY, Liew YJ, Lehnert EM, Michell CT, et al. The genome of *Aiptasia*, a sea anemone model for coral symbiosis. Proc Natl Acad Sci. 2015;112:11893–8.
21. Caron JB, Jackson DA. Taphonomy of the greater phyllopod bed community, burgess shale. Palaios. 2006;21:451–65.
22. Guerette PA, Hoon S, Seow Y, Raida M, Masic A, Wong FT, et al. Accelerating the design of biomimetic materials by integrating RNA-seq with proteomics and materials science. Nat Biotechnol. 2013;31:908–15.
23. Haiko J, Westerlund-Wikström B. The role of the bacterial flagellum in adhesion and virulence. Biology (Basel). 2013;2:1242–67.
24. Morales-García AL, Bailey RG, Jana S, Burgess JG. The role of polymers in cross-kingdom bioadhesion. Philos Trans R Soc B Biol Sci. 2019;374:20190192.
25. Aldred N. Transdisciplinary approaches to the study of adhesion and adhesives in biological systems. Philos Trans R Soc B Biol Sci. 2019;374:20190191.
26. Wainwright DK, Kleinteich T, Kleinteich A, Gorb SN, Summers AP. Stick tight: suction adhesion on irregular surfaces in the northern clingfish. Biol Lett. 2013;9:1–5.
27. Federle W, Barnes WJP, Baumgartner W, Drechsler P, Smith JM. Wet but not slippery: boundary friction in tree frog adhesive toe pads. J R Soc Interface. 2006;3:689–97.
28. Favi PM, Yi S, Lenaghan SC, Xia L, Zhang M. Inspiration from the natural world: from bio-adhesives to bio-inspired adhesives. J Adhes Sci Technol. 2014;28:290–319.
29. Hennebert E, Maldonado B, Ladurner P, Flammang P, Santos R. Experimental strategies for the identification and characterization of adhesive proteins in animals: a review. Interface Focus. 2015;5:20140064.
30. von Byern J, Grunweld I, editors. Biological adhesive systems. Austria: Springer Wien New York; 2017.
31. Waite JH. Mussel adhesion – essential footwork. J Exp Biol. 2017;220:517–30.
32. Burkett JR, Wojtas JL, Cloud JL, Wilker JJ. A method for measuring the adhesion strength of marine mussels. J Adhes Dent. 2009;85:601–15.
33. Lengerer B, Pfaller K, Berezikov E, Ladurner P, Schärer L, Salvenmoser W, et al. Biological adhesion of the flatworm *Macrostomum lignano* relies on a duo-gland system and is mediated by a cell type-specific intermediate filament protein. Front Zool. 2014;11:12.
34. Hennebert E, Wattiez R, Flammang P. Characterisation of the carbohydrate fraction of the temporary adhesive secreted by the tube feet of the sea star *Asterias rubens*. Marine Biotechnol. 2011;13:484–95.
35. Hawthorn AC, Opell BD. Evolution of adhesive mechanisms in cribellar spider prey capture thread: evidence for van der Waals and hygroscopic forces. Biol J Linn Soc. 2002;77:1–8.
36. Betz O, Kölsch G. The role of adhesion in prey capture and predator defence in arthropods. Arthropod Struct Dev. 2004;33:3–30.
37. Zhao H, Sun C, Stewart RJ, Waite JH. Cement proteins of the tube-building polychaete *Phragmatopoma californica*. J Biol Chem. 2005;280:42938–44.
38. Jensen RA, Morse DE. The bioadhesive of *Phragmatopoma californica* tubes: a silk-like cement containing L-DOPA. J Comp Physiol B. 1988;158:317–24.
39. Hamel J-F, Mercier A. Cuvierian tubules in tropical holothurians: usefulness and efficiency as a defence mechanism. Mar Freshw Behav Physiol. 2000;33:115–39.
40. Hennebert E, Leroy B, Wattiez R, Ladurner P. An integrated transcriptomic and proteomic analysis of sea star epidermal secretions identifies proteins involved in defense and adhesion. J Proteomics. 2015;128:83–91.
41. Lehr CM. From sticky stuff to sweet receptors - achievements, limits and novel approaches to bioadhesion. Eur J Drug Metab Pharmacokinet. 1996;21:139–48.
42. Yu M, Deming TJ. Synthetic polypeptide mimics of marine adhesives. Macromolecules. 1998;31:4739–45.
43. Hiraishi N, Kaneko D, Taira S, Wang S, Otsuki M, Tagami J. Mussel-mimetic, bioadhesive polymers from plant-derived materials. J Investig Clin Dent. 2015;6:59–62.
44. Cui M, Ren S, Wei S, Sun C, Zhong C. Natural and bio-inspired underwater adhesives: current progress and new perspectives. APL Mater. 2017;5:116102.
45. Callow JA, Callow ME. Trends in the development of environmentally friendly fouling-resistant marine coatings. Nat Commun. 2011;2:244.
46. Imbesi PM, Finlay JA, Aldred N, Eller MJ, Felder SE, Pollack KA, et al. Targeted surface nanocomplexity: two-dimensional control over the composition, physical properties and anti-biofouling performance of hyperbranched fluoropolymer-poly (ethylene glycol) amphiphilic crosslinked networks. Polym Chem. 2012;3:3121–31.
47. Zhao Y, Wu Y, Wang L, Zhang M, Chen X, Liu M, et al. Bio-inspired reversible underwater adhesive. Nat Commun. 2017;8:1–8.

48. Sagert J, Sun C, Waite H. Chemical subtleties of mussel and polychaete holdfasts. In: Smith AM, Callow JA, editors. Biological adhesives. Berlin: Springer; 2006. p. 125–43.
49. Flammang P, Lambert A, Wattier E, Hennebert E. Protein phosphorylation: a widespread modification in marine adhesives. In. Savannah: Proceedings of the 32nd Annual Meeting of the Adhesion Society Inc; 2009. p. 18-20.
50. Flammang P, Lambert A, Bailly P, Hennebert E. Polyphosphoprotein-containing marine adhesives. J Adhes Dent. 2009;85:447–64.
51. Smith AM. Biological adhesives: Springer international Publishing; 2016.
52. Waite JH. Adhesion in byssally attached bivalves. Biol Rev. 1983;58:209–31.
53. Piggot AM, Sivaguru M, Sanford RA, Gaskins HR, Fouke BW. Change in zooxanthellae and mucocyte tissue density as an adaptive response to environmental stress by the coral, *Montastraea annularis*. Mar Biol. 2009;156: 2379–89.
54. Herman A, Tonk L, Hoegh-guldberg O, Fransolet D, Plumier J. Increased cell proliferation and mucocyte density in the sea anemone *Aiptasia pallida* recovering from bleaching. PLOS ONE. 2013;8:1–7.
55. Yamashita K, Kawaii S, Nakai M, Fusetani N. Larval behavioral, morphological changes, and nematocyte dynamics during settlement of actinulae of *Tubularia mesembryanthemum*, Allman 1871 (Hydrozoa: Tubulariidae). Biol Bull. 2003;204:256–69.
56. Cutress CE, Ross DM. The sea anemone *Calliactis tricolor* and its association with the hermit crab *Dardanus venosus*. J Zool. 1969;158:225–41.
57. Watson GM, Mire P. Stereocilia based mechanoreceptors of sea anemones. In: Lim DJ, editor. Cell and molecular biology of the ear. Boston: Springer US; 2000. p. 19–39.
58. Aldred N, Høeg JT, Maruzzo D, Clare AS. Analysis of the behaviours mediating barnacle cyprid reversible adhesion. PLoS One. 2013;8:e68085.
59. Autumn K, Liang Y, Hsieh S, Zesch W, Chan W, Kenny T, et al. Adhesive force of a single gecko foot-hair. Nature. 2000;405:681–5.
60. Kesel A, Martin A, Seidl T. Adhesion measurements on the attachment devices of the jumping spider *Evarcha arcuata*. J Exp Biol. 2003;206:2733–8.
61. Hennebert E, Viville P, Lazzaroni R, Flammang P. Micro- and nanostructure of the adhesive material secreted by the tube feet of the sea star *Asterias rubens*. J Struct Biol. 2008;164:108–18.
62. Phang IY, Aldred N, Clare AS, Vancso GJ. Towards a nanomechanical basis for temporary adhesion in barnacle cyprids (*Semibalanus balanoides*). J R Soc Interface. 2008;5:397–401.
63. Martin G. A new function of rhabdites: mucus production for ciliary gliding. Zeitschrift für Morphol der Tiere. 1978;91:235–48.
64. Hennebert E, Gregorowicz E, Flammang P, et al. Biol Open. 2018;7: bio037358.
65. Santos R, da Costa G, Franco C, Gomes-Alves P, Flammang P, Coelho A. First insights into the biochemistry of tube foot adhesive from the sea urchin *Paracentrotus lividus* (Echinoidea, Echinodermata). Marine Biotechnol. 2009: 686–98.
66. Lebesgue N, da Costa G, Ribeiro RM, Ribeiro-Silva C, Martins GG, Matranga V, et al. Deciphering the molecular mechanisms underlying sea urchin reversible adhesion: a quantitative proteomics approach. J Proteomics. 2016; 138:61–71.
67. Kamino K, Nakano M, Kanai S. Significance of the conformation of building blocks in curing of barnacle underwater adhesive. FEBS J. 2012;279:1750–60.
68. Ohkawa K, Nishida A, Yamamoto H, Waite JH. A glycosylated byssal precursor protein from the green mussel *Perna viridis* with modified dopa side-chains. Biofouling. 2004;20:101–15.
69. Abdel-fattah AF, Sary HH. Glycoproteins from *Ulva lactuca*. Phytochemistry. 1987;26:1447–8.
70. Lengerer B, Hennebert E, Flammang P, Salvenmoser W, Ladurner P. Adhesive organ regeneration in *Macrostomum lignano*. BMC Dev Biol. 2016;16:20.
71. Wunderer J, Lengerer B, Pjeta R, Bertemes P, Kremser L, Lindner H, et al. A mechanism for temporary bioadhesion. Proc Natl Acad Sci. 2019;116:4297–306.
72. Meikle P, Richards G, Yellowlees D. Structural determination of the oligosaccharide side chains from a glycoprotein isolated from the mucus of the coral *Acropora formosa*. J Biol Chem. 1987;262:16941–7.
73. Zayas RM, Cebrià F, Guo T, Feng J, Newmark PA. The use of lectins as markers for differentiated secretory cells in planarians. Dev Dyn. 2010;239: 2888–97.
74. Wang CS, Stewart RJ. Localization of the bioadhesive precursors of the sandcastle worm, *Phragmatopoma californica* (Fewkes). J Exp Biol. 2012;215: 351–61.
75. Hwang DS, Masic A, Prajatelistia E, Iordachescu M, Waite JH. Marine hydroid perisarc: a chitin- and melanin-reinforced composite with DOPA-iron (III) complexes. Acta Biomater. 2013;9:8110–7.
76. Paz MA, Fluckiger R, Boak A, Kagan HM, Gallop PM. Specific detection of quinoproteins by redox-cycling staining. J Biol Chem. 1991;266:689–92.
77. Candiano G, Bruschi M, Musante L, Santucci L, Ghiggeri GM, Carnemolla B, et al. Blue silver: a very sensitive colloidal Coomassie G-250 staining for proteome analysis. Electrophoresis. 2004;25:1327–33.
78. Deerinck T, Bushong E, Lev-Ram V, Shu X, Tsien R, Ellisman M. Enhancing serial block-face scanning electron microscopy to enable high resolution 3-D nanohistology of cells and tissues. Microsc Microanal. 2010;16:1138–9.

Publisher's Note